CHEMISTRY OF MATERIALS

Article

pubs.acs.org/cm

Mg/O_2 Battery Based on the Magnesium–Aluminum Chloride Complex (MACC) Electrolyte

Gulin Vardar,[†] Jeffrey G. Smith,[‡] Travis Thompson,[‡] Kouji Inagaki,[§] Junichi Naruse,[∥] Hidehiko Hiramatsu,[§] Alice E. S. Sleightholme,[⊥] Jeff Sakamoto,[‡] Donald J. Siegel,*[,‡,†,#] and Charles W. Monroe*[,▽]

[†]Materials Science and Engineering Department, [‡]Mechanical Engineering Department, and [⊥]Chemical Engineering Department, University of Michigan, Ann Arbor, Michigan 48109, United States

[§]Research Laboratories, DENSO Corporation, 500-1, Minamiyama, Komenoki-cho, Nisshin, 470-0111, Japan

[∥]North America Research & Development, DENSO International America, Inc., 24777 Denso Drive, Southfield, Michigan 48086, United States

[#]Department of Energy Conversion and Storage, Technical University of Denmark, Fysikvej, Building 309, 2800 Kongens Lyngby, Denmark

[▽]Department of Engineering Science, University of Oxford, Parks Road, Oxford OX1 3PJ, United Kingdom

Supporting Information

ABSTRACT: Mg/O_2 cells employing a $MgCl_2/AlCl_3$/DME (MACC/DME) electrolyte are cycled and compared to cells with modified Grignard electrolytes, showing that performance of magnesium/oxygen batteries depends strongly on electrolyte composition. Discharge capacity is far greater for MACC/DME-based cells, while rechargeability in these systems is severely limited. The Mg/O_2-MACC/DME discharge product comprises a mixture of $Mg(ClO_4)_2$ and $MgCl_2$, with the latter likely formed from slow decomposition of the former. The presence of Cl in these compounds suggests that the electrolyte participates in the cell reaction or reacts readily with the initial electrochemical products. A rate study suggests that O_2 diffusion in the electrolyte limits discharge capacities at higher currents. Formation of an insulating product film on the positive electrodes of Mg/O_2-MACC/DME cells following deep discharge increases cell impedance substantially and likely explains the poor rechargeability. An additional impedance rise consistent with film formation on the Mg negative electrode suggests the presence of detrimental O_2 crossover. Minimizing O_2 crossover and bypassing charge transfer through the discharge product would improve battery performance.

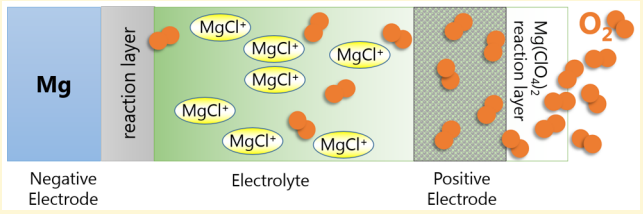

INTRODUCTION

Magnesium is an attractive negative-electrode material for battery applications due to its low cost, high energy density, and relative safety in comparison to alkali metals such as lithium.[1−10] Furthermore, across the many possible "metal/air" battery chemistries, the theoretical energy density provided by reacting Mg with O_2 is among the highest.[11,12] These advantages prompted the study of primary Mg/air batteries using aqueous electrolytes as early as the 1970s.[13−17] Despite decades of study since, several challenges remain.[18] For example, aqueous electrolytes corrode Mg electrodes because Mg reacts with H_2O spontaneously to form passivating $Mg(OH)_2$ on the electrode surface.[19] Thus, Mg/air batteries usually exhibit high interfacial impedance, making practical energy density at most a tenth of what theory suggests.[20] Also, the use of air as an O_2 source introduces pernicious impurities such as CO_2.

Relatively few studies have explored the possibility of a rechargeable Mg/O_2 cell based on a nonaqueous electrolyte and a pure O_2 gas source. Shiga et al. reported nonaqueous Mg/O_2 cells that operate at elevated temperatures.[21,22] The electrolytes employed included simple Mg salts such as $Mg(ClO_4)_2$ and $Mg(N(SO_2CF_3)_2)_2$ dissolved in organic solvents or ionic liquids. Due to their propensity for forming Mg^{2+}-impermeable passivation layers, it remains a matter of debate whether these electrolytes are compatible with Mg metal.[7,23] The present authors reported a room-temperature nonaqueous Mg/O_2 battery with an electrolyte based on a modified Grignard reagent.[24] This electrolyte was previously shown to allow for efficient Mg deposition/dissolution and exhibited high oxidative stability,[25] but the reversible energy density exhibited by Mg/O_2 cells based on it was low.[24]

It is well-known that Grignard reagents react vigorously with water and are pyrophoric.[26] Consequently, the development of less reactive electrolytes is an area of active research. One promising option is the all-inorganic magnesium aluminum

Received: June 19, 2016
Revised: October 3, 2016

DOI: 10.1021/acs.chemmater.6b02488
Chem. Mater. XXXX, XXX, XXX−XXX

chloride complex (MACC) reported by Doe et al.[27] MACC is synthesized by reacting a simple Mg salt with a Lewis acid in a nonaqueous solvent such as dimethoxyethane (DME) or tetrahydrofuran (THF). Electrochemical conditioning of the initially synthesized solution activates the electrochemical species responsible for reversible Mg deposition.[28−30] Conditioned MACC/DME allows Mg plating and stripping at room temperature with low deposition overpotentials (<300 mV vs $Mg/Mg^{2+/0}$), high Coulombic efficiency (>95%), and high oxidative stability (>3 V vs $Mg^{2+/0}$ with a Pt working electrode). In addition, the conductivity of MACC is relatively high (~2 mS/cm)[27] when compared to Grignard electrolytes (~0.3 mS/cm).[31] Although the exceptional properties exhibited by MACC suggest its promise for use in metal−air batteries, to our knowledge no reports of Mg/O_2 cells based on MACC/DME exist.

A high-capacity Mg/O_2 battery based on MACC/DME is reported here. This room-temperature Mg/O_2 cell exhibits a capacity similar to those of elevated-temperature cells based on simple Mg−salt electrolytes[21,22] yet is much higher than that of the room-temperature Mg/O_2 battery based on a modified Grignard electrolyte.[24] The discharge product of the MACC/DME Mg/O_2 cell is found to be a mixture of $Mg(ClO_4)_2$ and $MgCl_2$, which arises from slow decomposition of metastable $Mg(ClO_4)_2$ into $MgCl_2$. The presence of Cl points to undesirable electrolyte consumption during discharge-product formation.

In agreement with earlier studies using different electrolytes,[21,22] the rechargeability of the Mg/O_2-MACC/DME battery was found to be poor. This observation prompted additional characterization using electrochemical impedance spectroscopy (EIS) to identify factors that block reversal of the cell reaction. EIS shows that exposure to an O_2-saturated electrolyte accelerates film formation on Mg metal, leading to an impedance increase. In a Mg/O_2 cell, such an effect would arise from O_2 crossover to the negative electrode from the positive. In addition, EIS reveals a film resistance on the positive electrode that rises with depth of discharge, suggesting that the growth of an electrically insulating discharge product impedes cell performance. Ironically, the vastly larger quantity of discharge product produced in cells using MACC/DME (and associated electrode passivation) could explain the limited recharge capacity in comparison to cells based on the modified Grignard electrolyte.

The effects of discharge rate on capacity and discharge voltage were examined from 0.02 to 1 mA cm^{-2} (superficial). The results suggest that slow diffusion of O_2 in the electrolyte also contributes to limitations in discharge capacity at discharge currents above 0.1 mA cm^{-2}.

We conclude that efforts to improve the performance of nonaqueous Mg/O_2 cells should aim to (i) minimize O_2 crossover, (ii) bypass or improve charge transfer through the discharge product, and (iii) identify cathode/electrolyte combinations that are highly permeable to O_2.

METHODS

Experimental Section. Mg/O_2 cycling experiments were performed using cells designed for metal/O_2 testing, depicted in the Supporting Information Figure S1. Cell fabrication and disassembly closely followed the procedures described earlier by Griffith et al.[32] Mg/O_2 cells (EL-CELL Gmbh, Germany) were assembled by sandwiching a glass-fiber separator (0.5 mm thick, EL-CELL Gmbh, Germany) between a planar metallic−Mg negative electrode (99.9%, Goodfellow, U.S.A.) and a porous-carbon positive electrode (26 mg, SIGRACET GDL 24 BC, Ion Power, Inc., U.S.A.). A stainless-steel plate with 1.5 mm diameter perforations (EL-CELL Gmbh, Germany) acted as a positive current collector and was coated with evaporatively deposited Pt to impede corrosion during testing. The perforations in the plate allowed contact between the carbon and stagnant O_2 (99.993%, Cryogenic Gases, U.S.A.; 2 bar absolute). The separator and carbon were saturated with an electrolyte comprising $MgCl_2$ (99.99%, Sigma-Aldrich, U.S.A.) and $AlCl_3$ (99.999%, Sigma-Aldrich, U.S.A.) in DME (99.5%, anhydrous, Sigma-Aldrich, U.S.A.), referred to above as MACC/DME. The electrolyte was produced using the precursor materials and conditioned to achieve high performance (cf. Figures S2−S4) via batch electrolysis (i.e., holding at a negative potential 500 mV below the Mg deposition overpotential until cyclic voltammetry showed the Coulombic efficiency for Mg plating/stripping to be >96%). Discharge experiments were performed at room temperature using a series 4000 battery tester (Maccor, U.S.A.). To probe the discharge mechanism, the discharge product was characterized by scanning electron microscopy (SEM), energy dispersive X-ray spectroscopy (EDS), X-ray diffraction (XRD), Raman spectroscopy (RS), Auger electron spectroscopy (AES), and X-ray photoelectron spectroscopy (XPS). Additional details are provided in the Supporting Information.

Computational Details. Density functional theory calculations (VASP code)[33−35] were used to characterize the electronic structure of $Mg(ClO_4)_2$ and $MgCl_2$ and to estimate the enthalpy and free-energy changes associated with the decomposition reaction hypothesized to accompany discharge (described below). Blochl's projector augmented wave (PAW) method[36] was used to treat the core/valence electron interaction. The generalized gradient approximation (GGA) expressed with the formulation of Perdew−Burke−Ernzerhof (PBE)[37] was used for the exchange-correlation energy. Additional calculations were preformed using van der Waals-aware functionals.[38−40] The Brillouin zone was sampled with a Γ-centered *k*-point mesh with density 12 × 12 × 6 for $Mg(ClO_4)_2$ and 12 × 3 × 12 for $MgCl_2$. Lattice constants were determined by relaxing the cell shape, volume, and atom positions. A plane-wave cutoff energy of 520 eV and a force tolerance of 0.04 eV/Å was used for all geometry optimizations. The ground state energy of the O_2 molecule was evaluated using spin-polarized calculations.

RESULTS AND DISCUSSION

Electrochemical Testing. Figure 1 shows representative discharge curves for the MACC/DME-based Mg/O_2 cell at six discharge rates ranging from 0.02 to 1 mA cm^{-2} (superficial). The open-circuit (OC) voltage prior to discharge (2.0 ± 0.1 V) is similar to the voltage reported previously for other nonaqueous Mg/O_2 cells.[21,24] In an earlier report the authors argued that an OC voltage of ~2.0 V results from the half-reaction associated with superoxide formation at the positive electrode, since O_2^- forms from O_2 at ~2 V vs Mg/Mg^{2+}.[24] Control experiments in which the cells were not exposed to O_2 showed negligible capacity (Figure S5), suggesting that the presence of O_2 is necessary for discharge to occur.

The cell based on MACC/DME exhibits a capacity of ~400 μAh cm^{-2} at a discharge rate of 50 μAcm^{-2}. (This corresponds to a specific capacity of ~38 mAh $g_{cathode}^{-1}$.) In contrast, the capacity reported previously for a similar Mg/O_2 cell using the 4:1 $(PhMgCl)_4$-$Al(OPh)_3$/THF) modified Grignard electrolyte was much lower, ~13 μAh cm^{-2}, at 1/10 the discharge rate (5 μA cm^{-2}).[24]

The large difference in capacities between cells based on Grignard/THF and MACC/DME owes at least partially to the higher conductivity of the MACC solution and the higher solubility of O_2 in DME. Indeed, O_2 permeability (defined as the product of saturated O_2 concentration and effective diffusivity) is thought to contribute to capacity limitations in

DOI: 10.1021/acs.chemmater.6b02488
Chem. Mater. XXXX, XXX, XXX−XXX

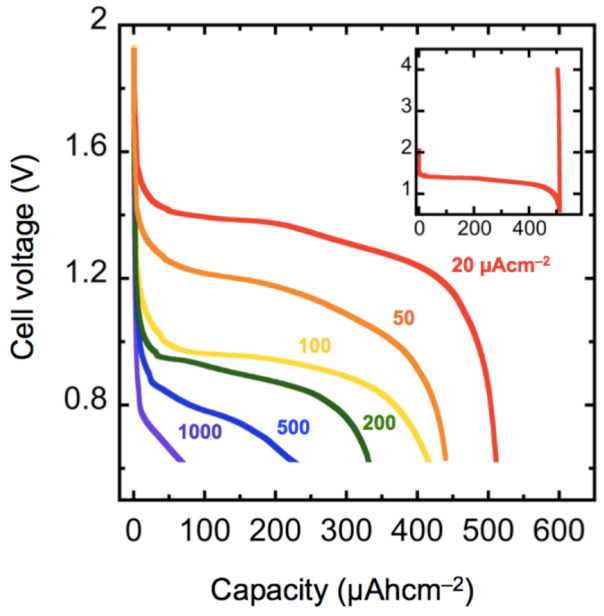

Figure 1. Cell voltage vs capacity for Mg/O_2 cells at current densities ranging from 0.02 to 1 mA cm^{-2} (superficial). The inset shows a typical discharge/charge cycle at 0.02 mA cm^{-2}.

Li/O_2 batteries.[32,41] The conductivity of the modified Grignard electrolyte examined previously was reported to be 1.24 mS cm^{-1},[25] whereas the conductivity of the conditioned MACC/DME was 2.21 mS cm^{-1}. The latter value agrees with the ~2 mS cm^{-1} reported by Doe et al.[27] Furthermore, the solubility of O_2 in DME has been reported to be 5 times higher than in THF.[42,43] Taken together, these data support the notion that differences in oxygen permeability between the electrolytes can be associated with the observed differences in capacity at higher operating rates. Additional tuning of the electrolyte composition could raise the capacities observed for Mg/O_2 systems. For example, varying the donor number of the solvent appears to have a significant effect on the capacity of nonaqueous Li/O_2 cells.[44]

Recharging at 0.02 mA cm^{-2} yielded negligible recharge capacity before the cutoff voltage of 4 V vs Mg/Mg^{2+} was reached (cf. Figure 1 inset). This response of the Mg/O_2-MACC/DME cells differs substantially from the behavior observed previously for Mg/O_2-Grignard/THF cells, which exhibited some rechargeability, albeit at low recharge rates (5 μA cm^{-2}).[24] Possible explanations for this distinct behavior are discussed in conjunction with the EIS results below.

Discharge-Product Characterization. Figure 2 shows SEM images of positive (carbon) electrodes harvested from Mg/O_2-MACC/DME cells. Figure 2a shows an electrode after first discharge, which is covered with discharge product only on the side closest to the O_2 inlet. This product was absent from a control electrode (inset of Figure 2b) held under oxygen at OC (i.e., galvanostatically at 0 A) for the same time period. Higher-magnification images in Figure 2b reveal that the product comprises faceted particles. The much higher capacity of MgO_2-MACC/DME cells compared to MgO_2-Grignard cells is reflected by the much larger amount of discharge product visible on the electrode following discharge. Figure S10 compares SEM images of carbon electrodes that were recorded after discharge using MACC/DME and the modified Grignard electrolyte. The electrode from the MACC/DME cell exhibits high surface coverage by the product, which extends beyond

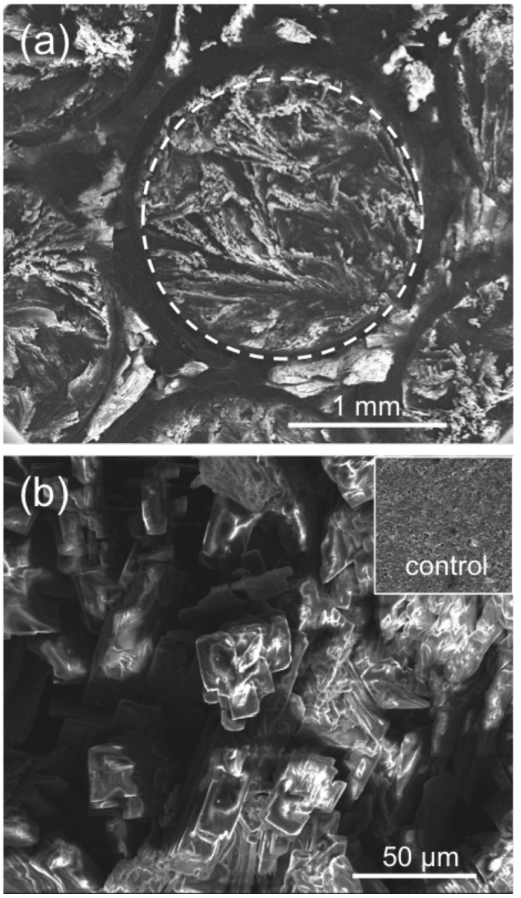

Figure 2. (a) SEM image of the positive-electrode surface on the side closest to the O_2 gas inlet after first discharge (0.05 $mAcm^{-2}$). The dashed circle represents the boundary of the region that was directly exposed to O_2 through perforations in the Pt-coated current collector. (b) Higher magnification of the electrode after first discharge, with an inset image of a control electrode exposed to O_2 in a similar cell held at open circuit for the same period.

the boundaries of the perforations in the current collector (these perforations allow direct contact between C and O_2); in contrast, the electrode from the modified Grignard-based cell exhibits a single incomplete layer of product only on the portion of the carbon surface that was in contact with O_2.

The discharge-product composition was characterized using XRD, EDS, AES, and XPS. Figure 3a shows XRD patterns collected from the positive electrode at the end of a discharge at 50 μAcm^{-2} and for a control electrode held at OC for the same period. At the end of discharge, peaks associated with $MgCl_2$ and $Mg(ClO_4)_2$ are clearly present in the diffraction pattern from the positive electrode.

Figure 3b presents EDS spectra collected from two different spots on the discharge-product layer. The EDS data qualitatively confirms that the discharge product is rich in Cl and indicates some degree of spatial nonuniformity. RS, AES, and XPS (Figures S11 and S12) also confirm the spatial nonuniformity. RS shows that peaks for $MgCl_2$ and $Mg(ClO_4)_2$ can be observed in different locations on parts of the electrode surface covered by discharge product. Similarly, Mg $KL_{2,3}L_{2,3}$ AES spectra and Mg 2p XPS spectra collected from different spots on the discharge product show that the binding energies vary with respect to location. Taken together, these data suggest that the discharge product comprises a mixture of

DOI: 10.1021/acs.chemmater.6b02488
Chem. Mater. XXXX, XXX, XXX−XXX

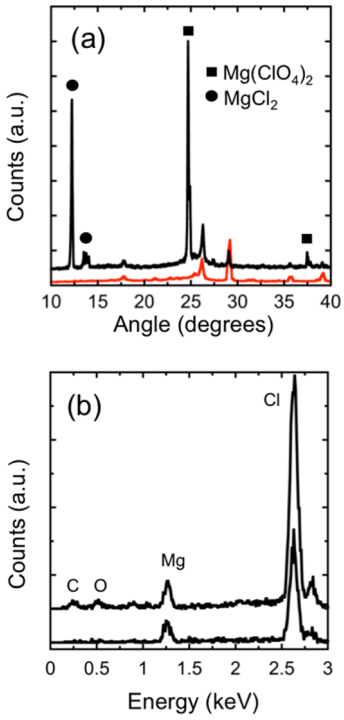

Figure 3. (a) XRD patterns of a discharged cathode (black) and a control cathode (red). Unlabeled peaks correspond to the carbon positive electrode. (b) EDS spectra collected in spot mode from two locations on the discharge product.

$Mg(ClO_4)_2$ and $MgCl_2$. Anhydrous $Mg(ClO_4)_2$ is believed to decompose spontaneously into $MgCl_2$ and O_2 at room temperature via the reaction[45]

$$Mg(ClO_4)_2 \rightarrow MgCl_2 + 4O_2 \quad (1)$$

Thus, the nonuniform product observed could be explained by electrochemical $Mg(ClO_4)_2$ formation, which is followed by gradual chemical decomposition into $MgCl_2$ and O_2.

DFT Calculations. Density functional theory calculations were preformed to evaluate the energetics of $Mg(ClO_4)_2$ decomposition via eq 1. The calculated enthalpy and free energy of reaction are $\Delta H_r = -42.6$ kJmol^{-1} and $\Delta G_r = -285.7$ kJ/mol, respectively, indicating that the decomposition of magnesium perchlorate into magnesium chloride should be spontaneous. Additional details regarding the DFT calculations can be found in the Supporting Information, Tables S1 and S2.

The discharge-product composition in Mg/O_2-MACC/DME cells differs from the mixed MgO/MgO_2 product previously observed in cells based on a modified Grignard electrolyte.[24] Nevertheless, the formation of Cl−O complexes has been observed in aqueous Mg/air chemistries using NaCl electrolytes.[46] Computational studies suggest that conditioned MACC/DME electrolyte contains chloromagnesium cations such as $MgCl^+$ and $Mg_2Cl_3^+$.[47] In principle, these species could react chemically with electrochemically formed O_2^- to produce $Mg(ClO_4)_2$. Such a reaction would be consistent with the observed discharge voltages shown in Figure 1. Both $Mg(ClO_4)_2$ and $MgCl_2$ are expected to be insulators, so sluggish electron transport through them could limit rechargeability.[48,49] Indeed, GGA-DFT calculations confirm that $MgCl_2$ and $Mg(ClO_4)_2$ are both insulators with large bandgaps of 5.6 and 5.3 eV, respectively. (Since semilocal functionals such as the GGA tend to underestimate bandgaps, these calculations probably represent lower bounds to the true bandgaps. Figure S13 shows the density of states for each compound.)

The presence of Cl in the discharge product indicates that electrolyte is consumed during or immediately after the electrochemical discharge reaction step.[50] Most Mg−halogen compounds have Gibbs free energies of formation similar to, or more negative than, that of MgO ($MgCl_2$: −592 kJmol^{-1}, MgF_2: −1071 kJmol^{-1}, $MgBr_2$: −504 kJmol^{-1}, MgO: −568 kJmol^{-1}).[51] Thus, it is likely that Cl, F, or Br in the electrolyte could be incorporated into the discharge product of a Mg/O_2 battery. For future studies, it is recommended that halogen-free electrolytes be explored.

Electrochemical Impedance Spectroscopy. The evolution of internal resistance was studied using EIS to explore the limited rechargeability of MACC/DME cells. Figure 4a shows Nyquist plots for a symmetric Mg/Mg cell with a 0.5 mm thick glass-fiber separator soaked with MACC/DME electrolyte and operated under Ar. The cell was kept at OC for a total of 3 h, during which an impedance spectrum was gathered every 10 min to examine temporal changes in the resistance of the Mg/electrolyte interface. The first EIS measurement (corresponding

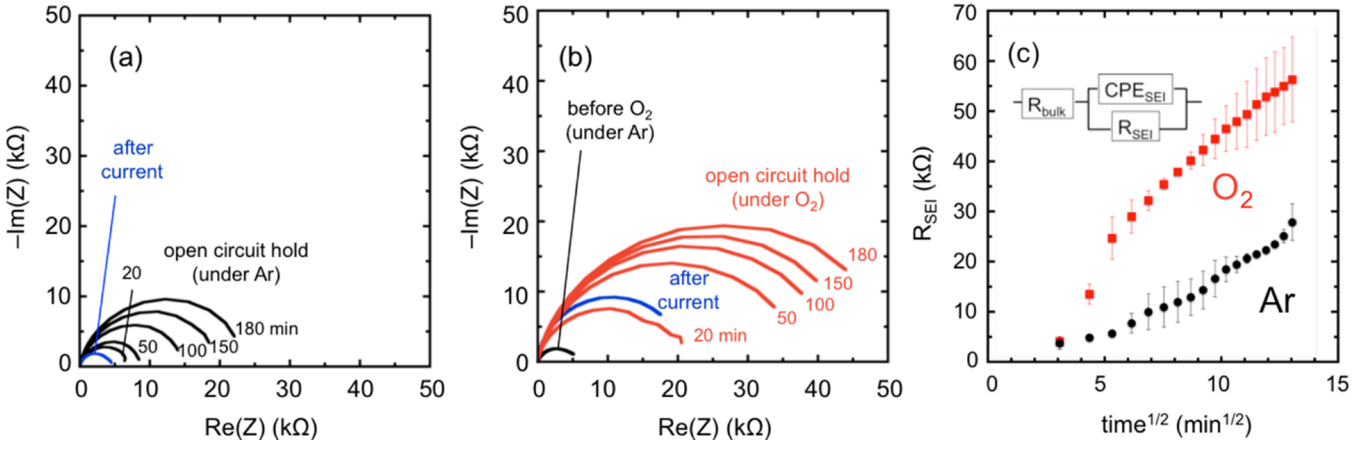

Figure 4. (a) Nyquist plots for a Mg/Mg cell containing MACC/DME electrolyte under Ar at various times during an OC hold (black) and after passing 0.075 mAh cm^{-2} through the cell at 0.05 mA cm^{-2} (blue). (b) Nyquist plots for a Mg/Mg cell using MACC/DME before O_2 exposure (black), under O_2 at various times after O_2 exposure during an OC hold (red), and after passing 0.075 mAh cm^{-2} (blue). (c) Equivalent-circuit-model fit for R_{SEI} during OC holds for Mg/Mg cells under Ar (black circles) and under O_2 (red squares).

DOI: 10.1021/acs.chemmater.6b02488
Chem. Mater. XXXX, XXX, XXX−XXX

to time = 0 min) was recorded less than 5 min after the cell was assembled.

A Nyquist plot produced from the Mg/Mg cell under Ar shows a single depressed semicircle. Depressed semicircles are often observed in battery impedance studies and are commonly attributed to electrode surface roughness.[52] The radius of the semicircle grows as a function of time, indicating an impedance increase arising from the formation of a partially passivating phase on the electrode surfaces. This behavior is similar to that observed for solid-electrolyte interphase (SEI) formation in Li-ion battery negative electrodes. After the 3 h OC hold, 0.075 mAh cm^{-2} of charge (a 1.5 h discharge at 0.05 mA cm^{-2}) was passed through the cell and another impedance spectrum was recorded (shown as the blue curve in Figure 3a). The interfacial impedance decreased substantially after current was applied, suggesting electrochemically driven dissolution of an SEI-like layer from the Mg electrode surfaces.

Contributions to the impedance associated with dissolved O_2 in the electrolyte were probed using a symmetric Mg/Mg cell exposed to O_2, rather than Ar, during the OC hold, for which Nyquist plots are shown in Figure 4b. The black curve represents an impedance spectrum collected before O_2 exposure, which is similar to the data in Figure 4a. In contrast to the Ar-only cell, the impedance of the cell exposed to O_2 is larger and grows more rapidly. The subsequent passage of 0.075 mAh cm^{-2} at 0.05 mA cm^{-2} results in an impedance decrease, but the cell does not return to its state before O_2 exposure.

To quantify the effects of O_2 exposure, an equivalent-circuit model (ECM), illustrated in Figure 4c, was used to fit the EIS data gathered from both the Ar- and O_2-exposed Mg/Mg cells. In the ECM, R_{bulk}, R_{SEI}, and CPE_{SEI} represent the bulk resistance associated with the electrolyte and the Mg electrode's interfacial resistance and equivalent capacitance, respectively. (A more complex ECM was also considered, which included uncompensated resistance and cell capacitance elements. This was found to increase the variances in the parameters without improving goodness-of-fit; additional details can be found in the Supporting Information.)

Figure 4c shows how R_{SEI} varies with respect to the square root of time for Mg/Mg-MACC/DME cells under Ar and O_2. An increase in R_{SEI} is expected to correlate with the growth of an SEI-like film. Notably, R_{SEI} increases with time under both Ar and O_2 atmospheres. Nevertheless, the cell exposed to O_2 exhibits a more rapid rate of increase and higher overall interfacial resistance, possibly due to oxidation of the Mg surface caused by the presence of O_2. Interestingly, R_{SEI} increases approximately linearly with the square root of time in both cases, suggesting a diffusion-limited film-growth process (Figure S7).

The evolution of R_{bulk}, which is associated with the resistance of the electrolyte and given by the high-frequency intercept of the Nyquist curve with the real axis, was investigated to gain insight into the relative stability of MACC and Grignard electrolytes under O_2. Comparison experiments, similar to those shown in Figure 4b, were performed on a Mg/Mg cell using the modified Grignard electrolyte.[24,25] As shown in Figure S8, the rate of increase and the absolute value of R_{bulk} were both larger for the modified Grignard electrolyte than for MACC/DME. Lower R_{bulk} values for MACC/DME confirm the earlier mentioned higher conductivity of MACC/DME. Furthermore, the lower rate of increase for R_{bulk} suggests that MACC/DME is more stable with respect to O_2 exposure than the Grignard electrolyte.

In addition to stability against chemical attack by O_2, the possible presence of O_2^- ions formed during cell discharge creates a strong oxidizing environment, which might be expected to further decompose electrolytes.[53−55] Stability in the specific presence of O_2 and its electrochemical products appears to be just as important as electrochemical stability against oxidation by the positive electrode—or even more important. These effects are illustrated by the full Mg/O_2 cell EIS data shown in Figure 5. During an initial OC hold under Ar, the Nyquist plot resembles that of the symmetric Mg/Mg cells (Figure 4a): there is only one apparent depressed semicircle. Similar to the symmetric Mg/Mg cells, exposure to O_2 results in an impedance increase. This could be attributed to SEI-like film formation on the Mg surface due to O_2 crossover from the positive electrode. The ECM depicted in Figure 4c was sufficient to model the impedance behavior of the Mg/O_2 cells up to this point (i.e., under OC conditions).

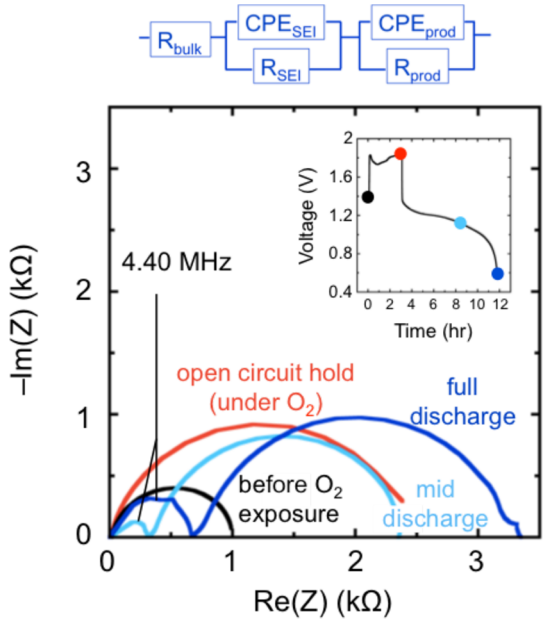

Figure 5. Electrochemical impedance spectra for a Mg/O_2 cell using MACC/DME electrolyte before O_2 exposure (black), after OC hold under O_2(red), mid-discharge (light blue), and after discharge (blue). The inset indicates the stage of (pre)discharge at which the EIS data was measured. The ECM used to model the spectra is shown above.

Upon discharge of the full Mg/O_2 cell (Figure 5, blue and light blue curves), a second depressed semicircle in the Nyquist plot appeared, presumably due to the formation of a new resistive interface in the cell. This likely owes to the formation of the discharge-product layer. Similar EIS data (showing a new semicircle after discharge) have been observed previously during discharge of Li/O_2 cells.[56]

An augmented ECM (Figure 5, top) containing an additional circuit element (parallel CPE_{prod}, R_{prod}) was used to model EIS data during and after discharge. Here, CPE_{prod} and R_{prod} represent the equivalent capacitance and resistance associated with the discharge-product layer. This layer's characteristic frequency is 4.40 MHz, with equivalent capacitance on the order of 1 pF. Both of these features point to the presence of a solid/liquid interphase.[57] Figure 5 also highlights that the size

DOI: 10.1021/acs.chemmater.6b02488
Chem. Mater. XXXX, XXX, XXX−XXX

of the new semicircle (which scales as R_{prod}) correlates with the depth of discharge. In contrast, the EIS data from Mg/O_2 cells using the modified Grignard electrolyte *do not* show the formation of a new semicircle upon discharge (see Figure S9). The absence of this feature—which was previously ascribed to the formation of a resistive discharge product—provides insight regarding the greater rechargeability noted for the Grignard electrolyte. In that system a mixed discharge product comprising MgO and MgO_2 was observed.[24] Both of these compounds were predicted to be insulators, similar to the $MgCl_2$ and $Mg(ClO_4)_2$ products found in the discharged MACC/DME cell.[58] Nevertheless, the discharge product in the Grignard-based cell covered only a fraction of the electrode surface. This behavior differs from the much higher coverages shown in Figure 2. Hence, the larger quantity of (insulating) discharge product present in the MACC/DME cell likely contributes to a higher product-film resistance, leading to limited rechargeability relative to the Grignard-based cell.

In summary, EIS measurements on symmetric Mg/Mg cells indicate that SEI-like film formation contributes to impedance at the Mg/electrolyte interface; moreover, the presence of O_2 accelerates the formation of these films. The EIS for full Mg/O_2 cells shows that growth of the discharge-product introduces a new and sizable interfacial resistance. The additional impedance contribution associated with the formation of a new interphase, arising from the low electrical conductivity of the discharge product and its high coverage on the electrode, likely explains the poor rechargeability of Mg/O_2 cells using MACC/DME.

Rate Dependence. In addition to energy density and rechargeability, rate capability is another important performance metric for batteries. The MACC/DME electrolyte allowed Mg/O_2 cells to be discharged at a wide range of current densities, ranging from 0.02 to 1 mA cm^{-2}. These compare to rates at which Li/O_2 cells have been tested, offering the possibility for a direct comparison of Li and Mg chemistries.

Figure 6 shows discharge capacity and cell voltage at 50% depth-of-discharge as functions of the discharge rate from 28 independently fabricated Mg/O_2 cells. The data shows (Figure 6a) that discharge rate does not significantly affect capacity at rates below 0.01 mA cm^{-2}. However, capacity decreases dramatically with increasing discharge rate at rates above 0.02 mA cm^{-2}. These characteristic features of the capacity vs rate curve are consistent with the model of Li/O_2 discharge presented by Liu and Monroe, which predicts that the capacity at higher rates falls as a power law with respect to discharge current.[41]

The higher-rate data were analyzed using Peukert's law, which is an empirical relation linking discharge capacity, q_{total}, and the discharge current density, i:[59]

$$\ln\left(\frac{q_{total}}{q_{ref}}\right) = (1-k)\ln\left(\frac{i}{i_{ref}}\right)$$

Here k is the Peukert exponent, i_{ref} is a reference current density (in this case, 1 mA cm^{-2}), and q_{ref} is the capacity at i_{ref}. The Peukert exponent, k, describes the ability of a battery to retain its capacity with increasing rate and can be compared across different battery chemistries. An ideal battery would have $k = 1$, meaning that the cell capacity is unchanged as a function of discharge rate. (For reference, k value for Li-ion batteries is 1.05,[60] whereas those of Pb/acid cells are nearer 1.4.[61]) Since drawing a current is associated with energy dissipation, $k > 1$. The capacities observed above 0.02 mA cm^{-2} for Mg/O_2 cells

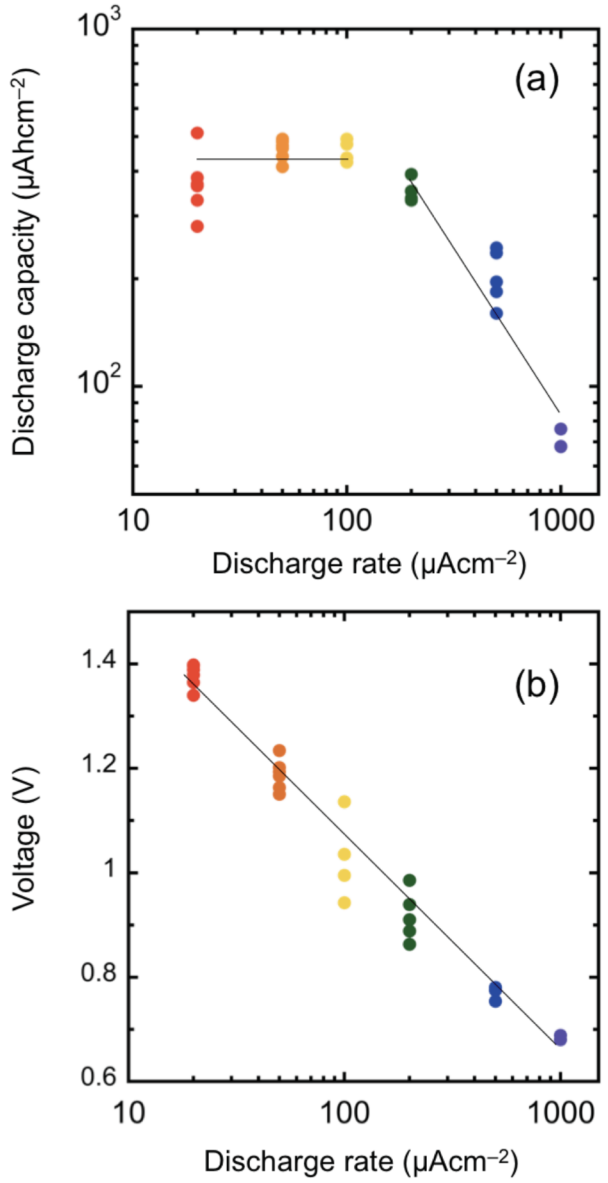

Figure 6. (a) Capacity per geometric electrode achieved at the 0.6 V cutoff potential as a function of discharge rate. Capacity falls as a power law with respect to discharge rate at rates higher than 0.02 mAh cm^{-2}. (b) Cell voltage at 50% depth-of-discharge as a function of discharge rate.

using MACC/DME follow a power-law dependence on the discharge current. The calculated Peukert exponent is 1.9, with a reference capacity of 91 μAh cm^{-2} at 1 mA cm^{-2}. This k value agrees well with the assumption that battery performance is limited by liquid-phase O_2 diffusion, which manifests as a Peukert exponent of 2.[41] Compared to the Li/O_2 chemistry, for which k = 1.6,[32] Mg/O_2 cells appear to exhibit lower rate capability. The transition from k = ~1 (below 0.01 mA cm^{-2}) to $k > 1$ (above 0.02 mA cm^{-2}) is commonly observed for metal/O_2 batteries; Liu and Monroe's model suggests that this transition occurs when the discharge current drives product formation sufficiently fast that O_2 is unable to diffuse all the way across the positive electrode.[41,62]

Figure 6b shows the cell potential at 50% depth-of-discharge as a function of discharge rate. Following an analysis similar to that of Viswanathan et al.,[63] the present data reveals a Tafel

DOI: 10.1021/acs.chemmater.6b02488
Chem. Mater. XXXX, XXX, XXX−XXX

slope of 4.9 V^{-1} and an exchange-current density of 1.6 μA cm^{-2} (superficial). Compared to Li/O_2 cells operated at the same rates (Tafel slope 11 ± 1 V^{-1} and exchange current density 7 ± 3 μA cm^{-2}), the present Mg/O_2 cells have a lower exchange-current density, suggesting that kinetic overpotentials are higher.

CONCLUSION

A nonaqueous Mg/O_2 cell based on the MACC/DME electrolyte was demonstrated and found to exhibit high discharge capacity but poor rechargeability. The discharge product was characterized using several techniques and was determined to be a mixture of crystalline $Mg(ClO_4)_2$ and $MgCl_2$. This combination is consistent with a discharge reaction that proceeds via initial reduction of O_2 to O_2^-, followed by chemical formation of $Mg(ClO_4)_2$ and its (slow) partial decomposition into $MgCl_2$ and O_2. The presence of Cl in the discharge product suggests that the electrolyte participates in the discharge reaction. The MACC/DME cell yielded significantly higher capacity than a similar cell based on a modified Grignard/THF electrolyte.[24] This behavior is consistent with the larger quantity of discharge product visible on the surface of the MACC/DME positive electrode, which appears to cover most of the electrode surface, and with the higher oxygen solubility and conductivity of the MACC/DME system.

The low recharge capacity of the MACC/DME system motivated an impedance study on Mg/Mg symmetric cells and on full Mg/O_2 cells as a function of O_2 exposure and applied current. EIS measurements showed that the formation of an SEI-like film on Mg electrodes is accelerated by O_2 exposure. The application of current reduces the cell impedance, possibly by driving removal of the SEI-like layer. In full Mg/O_2 cells the formation of the discharge product layer contributes substantially to cell impedance and coincides with the appearance of a new semicircle in EIS measurements. This behavior reflects the insulating nature of the $Mg(ClO_4)_2/MgCl_2$ discharge product and the relatively large amount of product formed in the MACC/DME system. In contrast, a much smaller amount of discharge product was generated in a prior study using a modified Grignard electrolyte. These differences could explain the low rechargeability of the MACC/DME cells in comparison to the Grignard based systems. Redox mediators and cell designs that minimize O_2 crossover could be employed to promote rechargeability while maintaining large discharge capacities.

Finally, Mg/O_2 cells were discharged over a wide range of rates. The calculated Peukert exponent of 1.9 points to an O_2-diffusion-limited discharge regime at rates higher than 0.02 mA cm^{-2}. Compared to Li/O_2 cells, for which k = 1.6, the Mg/O_2 cells examined here exhibit lower rate capability.

ASSOCIATED CONTENT

Supporting Information

The Supporting Information is available free of charge on the ACS Publications website at DOI: 10.1021/acs.chemmater.6b02488.

Cell assembly, electrolyte and cell testing, additional characterization details, and density functional theory details (PDF)

AUTHOR INFORMATION

Corresponding Authors

*(D.J.S.) E-mail: djsiege@umich.edu.

*(C.W.M.) E-mail: charles.monroe@eng.ox.ac.uk.

Notes

The authors declare no competing financial interest.

ACKNOWLEDGMENTS

DENSO International America, Inc., provided financial support for this work. D.J.S. acknowledges the Villum Foundation's Visiting Professor Program, the Nordea Foundation's Residence Program, and DTU Energy for support during his stay at DTU. J.S. acknowledges partial support from the National Science Foundation, Grant CBET-1336387.

REFERENCES

(1) Aurbach, D.; Lu, Z.; Schechter, A.; Gofer, Y.; Gizbar, H.; Turgeman, R.; Cohen, Y.; Moshkovich, M.; Levi, E. Prototype systems for rechargeable magnesium batteries. *Nature* **2000**, *407*, 724−727.

(2) Yoo, H. D.; Shterenberg, I.; Gofer, Y.; Gershinsky, G.; Pour, N.; Aurbach, D. Mg rechargeable batteries: an on-going challenge. *Energy Environ. Sci.* **2013**, *6*, 2265−2279.

(3) Bucur, C. B.; Gregory, T.; Oliver, A. G.; Muldoon, J. Confession of a Magnesium Battery. *J. Phys. Chem. Lett.* **2015**, *6*, 3578−3591.

(4) Muldoon, J.; Bucur, C. B.; Gregory, T. Quest for nonaqueous multivalent secondary batteries: magnesium and beyond. *Chem. Rev.* **2014**, *114*, 11683−11720.

(5) Matsui, M. Study on electrochemically deposited Mg metal. *J. Power Sources* **2011**, *196*, 7048−7055.

(6) Watkins, T.; Kumar, A.; Buttry, D. A. Designer Ionic Liquids for Reversible Electrochemical Deposition/Dissolution of Magnesium. *J. Am. Chem. Soc.* **2016**, *138*, 641−650.

(7) Vardar, G.; Sleightholme, A. E.; Naruse, J.; Hiramatsu, H.; Siegel, D. J.; Monroe, C. W. Electrochemistry of magnesium electrolytes in ionic liquids for secondary batteries. *ACS Appl. Mater. Interfaces* **2014**, *6*, 18033−19039.

(8) Kumar, N.; Siegel, D. J. Interface-Induced Renormalization of Electrolyte Energy Levels in Magnesium Batteries. *J. Phys. Chem. Lett.* **2016**, *7*, 874−881.

(9) MacFarlane, D. R.; Forsyth, M.; Howlett, P. C.; Kar, M.; Passerini, S.; Pringle, J. M.; Ohno, H.; Watanabe, M.; Yan, F.; Zheng, W.; Zhang, S.; Zhang, J. Ionic liquids and their solid-state analogues as materials for energy generation and storage. *Nat. Rev. Mats.* **2016**, *1*, 15005.

(10) Shterenberg, I.; Salama, M.; Gofer, Y.; Levi, E.; Aurbach, D. The challenge of developing rechargeable magnesium batteries. *MRS Bull.* **2014**, *39*, 453−460.

(11) Zu, C.-X.; Li, H. Thermodynamic analysis on energy densities of batteries. *Energy Environ. Sci.* **2011**, *4*, 2614−2624.

(12) Radin, M. D.; Siegel, D. J. Non-Aqueous Metal-Air Batteries: Past, Present, and Future. In *Rechargeable Batteries: Materials, Technologies and New Trends*; Zhang, Z., Zhang, S. S., Eds.; Springer: Switzerland, 2015; pp 511−539.

(13) Hamlen, R. P.; Jerabek, E. C.; Ruzzo, J. C.; Siwek, E. G. Anodes for Refuelable Magnesium-Air Batteries. *J. Electrochem. Soc.* **1969**, *116*, 1588−1592.

(14) Sathyanarayana, S.; Munichandraiah, N. A new magnesium-air cell for long-life applications. *J. Appl. Electrochem.* **1981**, *11*, 33−39.

(15) Li, W.; Li, C.; Zhou, C.; Ma, H.; Chen, J. Metallic magnesium nano/mesoscale structures: their shape-controlled preparation and mg/air battery applications. *Angew. Chem., Int. Ed.* **2006**, *45*, 6009−6012.

(16) Ma, Y.; Li, N.; Li, D.; Zhang, M.; Huang, X. Performance of Mg−14Li−1Al−0.1Ce as anode for Mg-air battery. *J. Power Sources* **2011**, *196*, 2346−2350.

(17) Winther-Jensen, B.; Gaadingwe, M.; Macfarlane, D. R.; Forsyth, M. Control of magnesium interfacial reactions in aqueous electrolytes

DOI: 10.1021/acs.chemmater.6b02488
Chem. Mater. XXXX, XXX, XXX−XXX

towards a biocompatible battery. *Electrochim. Acta* **2008**, *53*, 5881−5884.
(18) Chen, L. D.; Nørskov, J. K.; Luntz, A. C. Theoretical Limits to the Anode Potential in Aqueous Mg−Air Batteries. *J. Phys. Chem. C* **2015**, *119*, 19660−19667.
(19) Song, G.; Atrens, A. Understanding Magnesium Corrosion—A Framework for Improved Alloy Performance. *Adv. Eng. Mater.* **2003**, *5*, 837−858.
(20) Zhang, T.; Tao, Z.; Chen, J. Magnesium−air batteries: from principle to application. *Mater. Horiz.* **2014**, *1*, 196−206.
(21) Shiga, T.; Hase, Y.; Kato, Y.; Inoue, M.; Takechi, K. A rechargeable non-aqueous Mg-O2 battery. *Chem. Commun. (Cambridge, U. K.)* **2013**, *49*, 9152−9154.
(22) Shiga, T.; Hase, Y.; Yagi, Y.; Takahashi, N.; Takechi, K. Catalytic Cycle Employing a TEMPO−Anion Complex to Obtain a Secondary Mg−O2Battery. *J. Phys. Chem. Lett.* **2014**, *5*, 1648−1652.
(23) Lu, Z.; Schechter, A.; Moshkovich, M.; Aurbach, D. On the electrochemical behavior of magnesium electrodes in polar aprotic electrolyte solutions. *J. Electroanal. Chem.* **1999**, *466*, 203−217.
(24) Vardar, G.; Nelson, E. G.; Smith, J. G.; Naruse, J.; Hiramatsu, H.; Bartlett, B. M.; Sleightholme, A. E. S.; Siegel, D. J.; Monroe, C. W. Identifying the Discharge Product and Reaction Pathway for a Secondary Mg/O2 Battery. *Chem. Mater.* **2015**, *27*, 7564−7568.
(25) Nelson, E. G.; Brody, S. I.; Kampf, J. F.; Bartlett, B. M. A Magnesium Tetraphenylaluminate Battery Electrolyte Exhibits a Wide Electrochemical Potential Window and Reduces Stainless Steel Corrosion. *J. Mater. Chem. A* **2014**, *2*, 18194−18198.
(26) Silverman, G. S.; Rakita, P. E. *Handbook of Grignard reagents*; Marcel Dekker: New York, 1996; p 708.
(27) Doe, R. E.; Han, R.; Hwang, J.; Gmitter, A. J.; Shterenberg, I.; Yoo, H. D.; Pour, N.; Aurbach, D. Novel, electrolyte solutions comprising fully inorganic salts with high anodic stability for rechargeable magnesium batteries. *Chem. Commun. (Cambridge, U. K.)* **2014**, *50*, 243−245.
(28) See, K. A.; Chapman, K. W.; Zhu, L.; Wiaderek, K. M.; Borkiewicz, O. J.; Barile, C. J.; Chupas, P. J.; Gewirth, A. A. The Interplay of Al and Mg Speciation in Advanced Mg Battery Electrolyte Solutions. *J. Am. Chem. Soc.* **2016**, *138*, 328−337.
(29) Barile, C. J.; Nuzzo, R. G.; Gewirth, A. A. Exploring Salt and Solvent Effects in Chloride-Based Electrolytes for Magnesium Electrodeposition and Dissolution. *J. Phys. Chem. C* **2015**, *119*, 13524−13534.
(30) Barile, C. J.; Barile, E. C.; Zavadil, K. R.; Nuzzo, R. G.; Gewirth, A. A. Electrolytic Conditioning of a Magnesium Aluminum Chloride Complex for Reversible Magnesium Deposition. *J. Phys. Chem. C* **2014**, *118*, 27623−27630.
(31) Guo, Y.; Yang, J.; NuLi, Y.; Wang, J. Study of electronic effect of Grignard reagents on their electrochemical behavior. *Electrochem. Commun.* **2010**, *12*, 1671−1673.
(32) Griffith, L. D.; Sleightholme, A. E.; Mansfield, J. F.; Siegel, D. J.; Monroe, C. W. Correlating Li/O2 cell capacity and product morphology with discharge current. *ACS Appl. Mater. Interfaces* **2015**, *7*, 7670−7678.
(33) Kresse, G.; Furthmüller, J. Efficient iterative schemes for ab initio total-energy calculations using a plane-wave basis set. *Phys. Rev. B: Condens. Matter Mater. Phys.* **1996**, *54*, 11169−11186.
(34) Kresse, G.; Hafner, J. Ab initio molecular dynamics for liquid metals. *Phys. Rev. B: Condens. Matter Mater. Phys.* **1993**, *47*, 558−561.
(35) Kresse, G.; Hafner, J. Ab initiomolecular-dynamics simulation of the liquid-metal−amorphous-semiconductor transition in germanium. *Phys. Rev. B: Condens. Matter Mater. Phys.* **1994**, *49*, 14251−14269.
(36) Blöchl, P. E. Projector augmented-wave method. *Phys. Rev. B: Condens. Matter Mater. Phys.* **1994**, *50*, 17953−17979.
(37) Perdew, J. P.; Burke, K.; Ernzerhof, M. Generalized Gradient Approximation Made Simple. *Phys. Rev. Lett.* **1996**, *77*, 3865−3868.
(38) Dion, M.; Rydberg, H.; Schroder, E.; Langreth, D. C.; Lundqvist, B. I. van der Waals density functional for general geometries. *Phys. Rev. Lett.* **2004**, *92*, 246401.
(39) Roman-Perez, G.; Soler, J. M. Efficient implementation of a van der Waals density functional: application to double-wall carbon nanotubes. *Phys. Rev. Lett.* **2009**, *103*, 096102.
(40) Klimeš, J.; Bowler, D. R.; Michaelides, A. Van der Waals density functionals applied to solids. *Phys. Rev. B: Condens. Matter Mater. Phys.* **2011**, *83*, 195131.
(41) Liu, J.; Khaleghi Rahimian, S.; Monroe, C. W. Capacity-limiting mechanisms in LiO2 batteries. *Phys. Chem. Chem. Phys.* **2016**, *18*, 22840−22851.
(42) Lu, Y.-C.; Kwabi, D. G.; Yao, K. P. C.; Harding, J. R.; Zhou, J.; Zuin, L.; Shao-Horn, Y. The discharge rate capability of rechargeable Li−O2 batteries. *Energy Environ. Sci.* **2011**, *4*, 2999−3007.
(43) Quaranta, M.; Murkovic, M.; Klimant, I. A new method to measure oxygen solubility in organic solvents through optical oxygen sensing. *Analyst* **2013**, *138*, 6243−6245.
(44) Johnson, L.; Li, C.; Liu, Z.; Chen, Y.; Freunberger, S. a.; Tarascon, J.-M.; Ashok, P. C.; Praveen, B. B.; Dholakia, K.; Bruce, P. G. The role of LiO2 solubility in O2 reduction in aprotic solvents and its consequences for Li−O2 batteries. *Nat. Chem.* **2014**, *6*, 1091−1099.
(45) Stern, K. H. High Temperature Properties and Decomposition of Inorganic Salts, Part 4. Oxy-Salts of the Halogens. *J. Phys. Chem. Ref. Data* **1974**, *3*, 481−526.
(46) Medeiros, M. G.; Dow, E. G. Magnesium-solution phase catholyte seawater electrochemical system. *J. Power Sources* **1999**, *80*, 78−82.
(47) Canepa, P.; Jayaraman, S.; Cheng, L.; Rajput, N. N.; Richards, W. D.; Gautam, G. S.; Curtiss, L. A.; Persson, K. A.; Ceder, G. Elucidating the structure of the magnesium aluminum chloride complex electrolyte for magnesium-ion batteries. *Energy Environ. Sci.* **2015**, *8*, 3718−3730.
(48) Radin, M. D.; Siegel, D. J. Charge transport in lithium peroxide: relevance for rechargeable metal−air batteries. *Energy Environ. Sci.* **2013**, *6*, 2370−2379.
(49) Radin, M. D.; Monroe, C. W.; Siegel, D. J. Impact of Space-Charge Layers on Sudden Death in Li/O2 Batteries. *J. Phys. Chem. Lett.* **2015**, *6*, 3017−3022.
(50) Kumar, N.; Radin, M. D.; Wood, B. C.; Ogitsu, T.; Siegel, D. J. Surface-Mediated Solvent Decomposition in Li−Air Batteries: Impact of Peroxide and Superoxide Surface Terminations. *J. Phys. Chem. C* **2015**, *119*, 9050−9060.
(51) NIST-JANAF Thermochemical Tables.
(52) Mulder, W. H.; Sluyters, J. H.; Pajkossy, T.; Nyikos, L. Tafel current at fractal electrodes. Connection with admittance spectra. *J. Electroanal. Chem. Interfacial Electrochem.* **1990**, *285*, 103−115.
(53) Leskes, M.; Moore, A. J.; Goward, G. R.; Grey, C. P. Monitoring the Electrochemical Processes in the Lithium-Air Battery by Solid State NMR Spectroscopy. *J. Phys. Chem. C* **2013**, *117*, 26929−26939.
(54) Ren, X.; Lau, K. C.; Yu, M.; Bi, X.; Kreidler, E.; Curtiss, L. A.; Wu, Y. Understanding side reactions in K-O2 batteries for improved cycle life. *ACS Appl. Mater. Interfaces* **2014**, *6*, 19299−192307.
(55) Schwenke, K. U.; Meini, S.; Wu, X.; Gasteiger, H. A.; Piana, M. Stability of superoxide radicals in glyme solvents for non-aqueous Li-O2 battery electrolytes. *Phys. Chem. Chem. Phys.* **2013**, *15*, 11830−11839.
(56) Zhang, T.; Zhou, H. A reversible long-life lithium-air battery in ambient air. *Nat. Commun.* **2013**, *4*, 1817.
(57) Irvine, J. T. S.; Sinclair, D. C.; West, A. R. Electroceramics Characterization by Impedance Spectroscopy. *Adv. Mater.* **1990**, *2*, 132−138.
(58) Smith, J. G.; Naruse, J.; Hiramatsu, H.; Siegel, D. J. Theoretical Limiting Potentials in Mg/O2 Batteries. *Chem. Mater.* **2016**, *28*, 1390−1401.
(59) Doerffel, D.; Sharkh, S. A. A critical review of using the Peukert equation for determining the remaining capacity of lead-acid and lithium-ion batteries. *J. Power Sources* **2006**, *155*, 395−400.
(60) Dubarry, M.; Liaw, B. Y. Identify capacity fading mechanism in a commercial $LiFePO_4$ cell. *J. Power Sources* **2009**, *194*, 541−549.
(61) Baert, D.; Vervaet, A. Lead-acid battery model for the derivation of Peukert's law. *Electrochim. Acta* **1999**, *44*, 3491−3504.

DOI: 10.1021/acs.chemmater.6b02488
Chem. Mater. XXXX, XXX, XXX−XXX

(62) Adams, B. D.; Radtke, C.; Black, R.; Trudeau, M. L.; Zaghib, K.; Nazar, L. F. Current density dependence of peroxide formation in the Li−O2 battery and its effect on charge. *Energy Environ. Sci.* **2013**, *6*, 1772−1778.
(63) Viswanathan, V.; Nørskov, J. K.; Speidel, A.; Scheffler, R.; Gowda, S.; Luntz, A. C. Li−O 2 Kinetic Overpotentials Tafel Plots from Experiment and First-Principles Theory. *J. Phys. Chem. Lett.* **2013**, *4*, 556−560.

DOI: 10.1021/acs.chemmater.6b02488
Chem. Mater. XXXX, XXX, XXX−XXX